

Transport in a Grooved Perfusion Flat-Bed Bioreactor for Cell Therapy Applications

Marc Horner, William M. Miller, J. M. Ottino, and E. Terry Papoutsakis*

Northwestern University, Department of Chemical Engineering, 2145 Sheridan Road E136, Evanston, Illinois 60208-3120

This study considers the transport of oxygen (a growth-associated solute) and lactate (a metabolic byproduct) in a flat-bed perfusion chamber modified to retain cells through the addition of grooves, perpendicular to the direction of flow, at the chamber bottom. The chamber has been successfully applied to hematopoietic cell culture and may be useful for other basic and applied biomedical applications. The objective of this study is to characterize the culture environment in terms of solute transport under various operational conditions. This will allow one to improve the design and operating strategy of the perfusion system for maximizing cell numbers. The system is numerically simulated using the finite element package FIDAP. The reaction kinetics describing oxygen uptake by cells are simplified to zero order to give an upper bound for the oxygen consumption. A flat-bed chamber without grooves is considered here as a benchmark. We show that the growth environment is not oxygen limited (local oxygen concentration above $10 \mu\text{M}$) for a variety of flow rates and culture conditions ($q_{O_2} = 0.1 \mu\text{mol}/(10^6 \text{ cells h})$). With a medium flow rate of $2.5 \text{ mL}/\text{min}$ through the reactor, the model predicts that the 29-cm^2 reactor can support at least 33.4×10^6 total cells when the inlet medium is in equilibrium with high (20%) oxygen concentration. The culture becomes oxygen limited however for the same flow rate for low (5%) oxygen concentration and can only support 7.2×10^6 total cells. Comparison of grooved vs nongrooved chambers reveals that the presence of grooves only affects solute transport on a local scale. This result is attributed to the small size ($200 \mu\text{m}$) of the cavities relative to the chamber dimensions. The comparison also yields an empirical relation that allows for rapid estimation of oxygen and lactate concentrations in the grooves using only the numerical simulation of the simpler nongrooved chamber. Finally, our investigation shows that, while decreasing the spacing between cavities decreases the total number of cells the reactor can support, the efficiency of the reactor is increased by 25% (on an area basis) without growth restriction.

Introduction

Cancer is the second leading cause of death in the United States, after heart disease. Cancer treatments target the most rapidly dividing cells in the body, i.e., the cancer cells. However, the bone marrow, the most rapidly dividing tissue (supplying 400 billion cells per day (1)) is concomitantly attacked. These treatments normally result in a nadir period of about 2 weeks, increasing patient risk for infection and bleeding. Clinical studies (2–4) suggest that ex vivo expanded hematopoietic cells have the potential to become a significant source of cells for hematopoietic (bone marrow) transplantation. The likely benefits of ex vivo expanded hematopoietic cell and gene therapies have been recently reviewed (5, 6).

Dexter et al. (7) described the first murine hematopoietic (bone-marrow) cultures. Moore and Sheridan (8) and Gartner and Kaplan (9) later adapted the Dexter protocol to human marrow culture. The discovery that more frequent medium changes increased total cell production and progenitor maintenance (10) ultimately led to the study of continuous perfusion systems. These reactor

systems maintain better-defined culture parameters, such as pH and (dissolved) oxygen concentration, continuously bathing the cells with nutrients and removing metabolic byproducts.

The first continuous perfusion systems were stromal-cell-dependent, demonstrating increased expansion of human cord-blood mononuclear cells (CB-MNC) (11) and bone marrow mononuclear cells (BM-MNC) (12, 13) over static controls. We have argued elsewhere (14) that ex vivo expansion of cells from peripheral blood (PB) (following stem-cell mobilization) and umbilical-cord blood (CB) for clinical applications would be significantly simplified if long-term hematopoietic culture (LTHC) did not require stroma. Similarly, ex vivo expansion of selected CD34^+ cells from all three sources (BM, PB, and CB) would be practically feasible only in stroma-free hematopoietic cultures. The perfusion chamber (Figure 1) currently being investigated by our group was shown to provide good colony-forming-unit granulocyte-macrophage (CFU-GM) expansion and long-term culture-initiating cell (LTC-IC) maintenance without stroma using the cytokines IL-3, IL-6, G-CSF, and SCF (14, 15). The perfusion chamber's grooves retain cells in the bioreactor in the presence of constant medium perfusion.

* To whom all correspondence should be addressed. Telephone: (847) 491-7455. Fax: (847) 491-3728. E-mail: e-paps@nwu.edu.

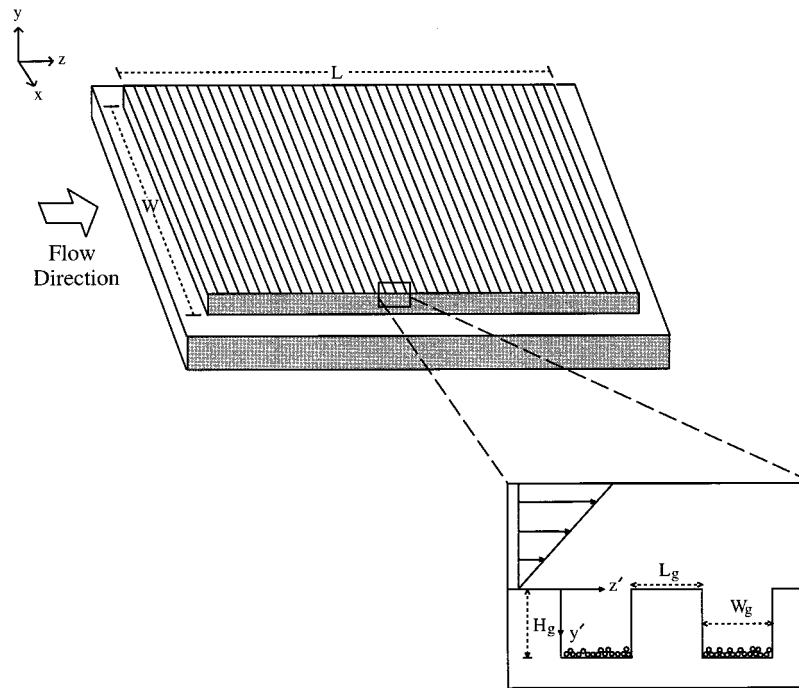


Figure 1. Model of the perfusion chamber, a flat-bed bioreactor in which a series of 190 grooves at the chamber bottom (shown in figure) retains cells in the presence of constant medium perfusion. This is a closed system, with no headspace when the lid is placed on top. Medium flows in the z -direction across the chamber. y' and z' represent the local coordinate system in a cavity.

The grooves also reduce mechanical stresses on the cells by isolating them from the primary flow. The simple design also allows for ease in harvesting at the end of the culture period; this is in direct contrast to hollow fiber systems where shell side cell harvests can be labor intensive (I). The growth environment generated in this chamber is reproducible and well-defined, a substantial advantage from the regulatory point of view.

A grooved-chamber design may also prove useful for basic biomedical studies of cells that do not attach firmly to surfaces (or to other cells) but need to be cultured under well-defined perfusion conditions. Thus, interactions between such cells and various surfaces or surface-attached cells can be examined.

A necessary condition for the successful use of this grooved-chamber design for either clinical or basic-study applications is the availability of a reliable transport model. Such a model will allow for estimation of the operational limits of a given geometrical design for a particular cell-culture application to ensure that cells are grown under nonlimiting culture conditions. The model would also allow the selection of suitable design characteristics and/or operational variables to achieve a desirable level of one or more culture parameters, such as dissolved oxygen, pH, and nutrient or byproduct concentrations.

Model Development

The culture system consists of three culture chambers in parallel ($14, 15$). The inner dimensions of each chamber, where the cells grow, are $3.81 \times 7.62 \times 0.5588$ ($W \times L \times 2H$) cm (see Figure 1 and Table 1). At the beginning of a culture, the starting hematopoietic cell population is seeded and mixed in each chamber (with medium) and allowed to settle for 15 min. The inlet flow is then slowly increased to the final flow rate over a period of 1.5 h. Cell culture proceeds for 5, 10, or 15 days, at which times the cells from each chamber are sequentially harvested.

Table 1. Constants Used in the Simulation Studies of the Perfusion Chamber

| parameter | value | ref |
|--------------------------------------|--|-----------------|
| chamber length (L) ^a | 7.62 cm | 14 |
| chamber width (W) ^a | 3.81 cm | 14 |
| chamber height ($2H$) ^a | 0.5588 cm | 14 |
| groove height (H_g) | 0.02 cm | 14 |
| groove width (W_g) | 0.02 cm | 14 |
| groove spacing (L_g) | 0.02 cm | 14 |
| medium viscosity | 0.6915×10^{-2} g/(cm s) | 37 |
| medium density | 0.993328 g/cm ³ | 38 |
| D_{O_2, H_2O} | 3.4×10^{-5} cm ² /s | 38 ^b |
| $C_{O_2, in}$ | 200 μ M | 18 |
| q_{O_2} | 0.01–0.025 μ mol/(10 ⁶ cells h) | 39 |
| | 0.03–0.1 μ mol/(10 ⁶ cells h) | 40 |
| K_{m, O_2} | O(1.0 μ M) | 19, 20 |
| $\langle r_{cell} \rangle$ | 5 μ m | 15 |
| D_{lac, H_2O} | 1.45×10^{-5} cm ² /s | 41 |
| q_{lac} | 0.05–0.4 μ mol/(10 ⁶ cells h) | 40 |

^a Inner dimensions. ^b Scaled using $D\mu/T = \text{constant}$.

The advection–diffusion of oxygen and lactate in a 2-D version of this bioreactor is considered here. The flow is steady-state and a pseudo-steady approach is taken for the mass transfer of the two model solutes (oxygen and lactate). Therefore, it is assumed that the average cell doubling time (~ 1 day) is long compared to the time required for establishment of steady-state species profiles.

The system is modeled in terms of the Navier–Stokes equation

$$\rho \left(\frac{\partial \mathbf{u}}{\partial t} + \mathbf{u} \cdot \nabla \mathbf{u} \right) \equiv -\nabla P + \mu \nabla^2 \mathbf{u} \quad (1)$$

and the species continuity equation for a dilute solution

$$\frac{\partial C}{\partial t} + \mathbf{u} \cdot \nabla C = D \nabla^2 C \quad (2)$$

Using the pseudo-steady-state and two-dimensional assumptions, the problem reduces to

$$\rho \left(v_y \frac{\partial v_y}{\partial y} + v_z \frac{\partial v_y}{\partial z} \right) = -\frac{\partial P}{\partial y} + \mu \left(\frac{\partial^2 v_y}{\partial y^2} + \frac{\partial^2 v_y}{\partial z^2} \right) \quad (3)$$

$$\rho \left(v_y \frac{\partial v_z}{\partial y} + v_z \frac{\partial v_z}{\partial z} \right) = -\frac{\partial P}{\partial z} + \mu \left(\frac{\partial^2 v_z}{\partial y^2} + \frac{\partial^2 v_z}{\partial z^2} \right) \quad (4)$$

whereas the solute balance for species i becomes

$$v_y \frac{\partial C_i}{\partial y} + v_z \frac{\partial C_i}{\partial z} = -D_{i,\text{med}} \left(\frac{\partial^2 C_i}{\partial y^2} + \frac{\partial^2 C_i}{\partial z^2} \right) \quad (5)$$

This solute balance is sequentially coupled to the hydrodynamic problem in the dilute solution limit.

A parabolic, i.e. well-developed, velocity profile is applied at the reactor inlet. This is justified by calculating the hydrodynamic entrance length for flow in a slit using

$$\frac{L_{\text{ent}}}{H} = aRe \quad (6)$$

where Re is the Reynolds number for Poiseuille flow

$$Re = \frac{\rho \langle v \rangle H}{\mu} \quad (7)$$

and a is a tolerance (indicating how close the center-line velocity is to the theoretical maximum), equal to 0.034 for 98% accuracy (16). Equation 7 predicts a 0.03-cm entrance length for the maximum flow rate considered here (2.5 mL/min). Since L_{ent} is less than 1% of the total reactor length, only the developing mass transfer is considered. Application of the no-slip condition to the reactor walls completes the hydrodynamic problem statement.

Estimation of Model Parameters. Parameter values utilized in the simulations are summarized in Table 1. The growth medium was assumed to have the properties of water at 37 °C. The decrease in solute diffusivity due to the presence of salts and albumin (17) is neglected. However, the reduction in oxygen solubility, primarily due to the presence of salts (18), is accounted for. A standard growth medium such as Dulbecco's modified Eagle's medium (DMEM) has a predicted oxygen concentration of 200 μM when in equilibrium with water-saturated air at 37 °C (18), and this value is used here. The medium reservoir is assumed well-mixed; therefore a constant, uniform concentration is applied at the inlet.

The effect of increasing total cell numbers throughout the culture period is examined in a pseudo-steady fashion. Cell numbers chosen were typical of three periods in the Sandstrom et al. (14, 15) studies: days 0–5 (2×10^6 total cells), day 10 (5×10^6 total cells), and day 15 (20×10^6 total cells); these time periods are referred to as early, middle, and late culture, respectively, in the rest of this paper. Dividing the number of cells at day 15 by the groove surface area ($WL/2$), we calculate that there are 1.38×10^6 cells/cm² groove. Assuming an average cell diameter of 10 μm , we expect there to be about 1.4 cell layers at the end of a culture. This is less than 10% of the groove height; therefore, we apply a heterogeneous reaction condition (as a boundary condition to the mathematical model) at the bottom of each cavity. The form of this boundary condition is based on a simplified Monod-type expression:

$$r_{O_2} = -D \frac{\partial C}{\partial y} \Big|_{y=-H_g} = \frac{r_{\text{max}} C}{K_{m,O_2} + C} \quad (8)$$

An upper bound of eq 8

$$r_{O_2} = -D \frac{\partial C}{\partial y} \Big|_{y=-H_g} = r_{\text{max}} \quad (9)$$

reduces the problem to zero-order kinetics. There are two reasons for this simplification. The first has to do with the low value of K_{m,O_2} , O(1 μM) (19, 20), relative to the inlet concentration. The second is to provide an upper bound for oxygen consumption in the reactor. Because of this simplification, we define an oxygen-restricted environment as one in which the local oxygen concentration is 10 times the K_{m,O_2} value.

An order of magnitude estimate for the effective reaction rate (r_{max}) is obtained by multiplying the specific reaction rate of a solute i (q_i) by the total cell number (N) and then dividing by the surface area for reaction ($WL/2$). The maximum values expected for the specific oxygen consumption rate ($q_{O_2} = -0.1 \mu\text{mol}/(10^6 \text{ cells h})$) and specific lactate production rate ($q_{\text{lac}} = +0.3 \mu\text{mol}/(10^6 \text{ cells h})$) are used here. Note that the product $q_i N$, and therefore r_{max} , is a function of time in a pseudo-steady-state sense. The volumetric flow rate (Q) is varied from 0.5 to 2.5 mL/min to examine the effect of nutrient availability.

Numerical Solution Methods. The differential system (eqs 3–5 plus boundary conditions) was solved using a computational fluid dynamics (CFD) code (FIDAP, Fluid Dynamics International, Inc., Evanston, IL). This finite element package implements a weighted residual method to solve for the velocity field and concentration distribution. The solute distribution in the grooved chamber is then compared to that of an equivalent cell culture chamber of the same dimension but that does not contain grooves. The nongrooved case is similar to the Graetz problem (21–23), which assumes that v_y is zero and also assumes a high (typically > 50) Péclet number, defined as

$$Pe = \frac{\langle v \rangle H}{D} \quad (10)$$

By comparison, the channel Péclet number is O(10^2) for the lowest flow rate considered here. Under the Graetz problem assumptions, the species continuity equation simplifies to

$$v_z \frac{\partial C_i}{\partial z} = -D_{i,\text{med}} \frac{\partial^2 C_i}{\partial y^2} \quad (11)$$

where v_z is the parabolic (Poiseuille) inlet profile

$$v_z = \frac{3}{4} \frac{Q}{WH} \left(1 - \frac{y^2}{H^2} \right) \quad (12)$$

Other boundary conditions are no-flux through the top ($y = H$) and a zero-order reaction at the slit bottom ($y = -H$). The rate of reaction is $r_{\text{max}}/2$ for this problem. This formulation is solved using the boundary element method (BEM) (24, 25) as described in the Appendix. This comparison is used not only to verify the CFD results but also to quantify the effect of introducing grooves (for cell retention) on the local solute concentration.

BEM and FIDAP results corresponding to oxygen consumption in a nongrooved chamber are compared in

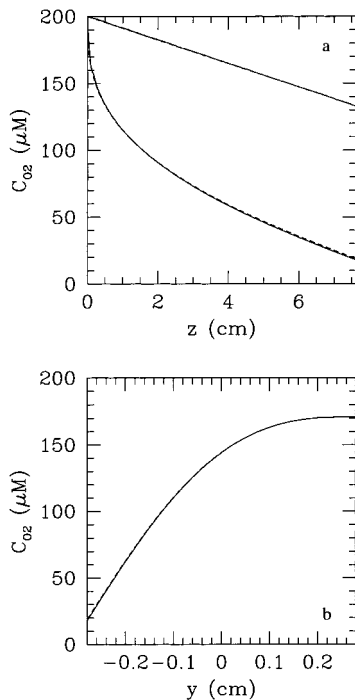


Figure 2. Comparison of BEM (dashed lines) and FIDAP (solid lines) results for transport in the flat-bed chamber showing good agreement in the axial (a) and radial (b) directions ($Q = 0.5$ mL/min, $q_{O_2}N = -2.0$ μ mol/h). The upper curves in a are the mixed-cup concentrations; the lower curves are the concentrations at the chamber bottom. The concentration profile across the chamber outlet is presented in b.

Figure 2. The difference between the axial and radial solute profiles, as well as the mixed-cup concentration ($\langle C \rangle$), defined as

$$\langle C \rangle = \frac{\int_{-H}^H C v_z dy}{\int_{-H}^H v_z dy} \quad (13)$$

is less than 1%. A flux balance on the reactor also closes to less than 1% error for this particular comparison, as well as for all other simulations presented here.

Results

Streamlines for the grooved perfusion chamber are shown in Figure 3. The inset depicts the cellular flow pattern present in each groove. The cellular flow is a direct result of fluid flow past an open cavity and has been considered extensively in the literature (26–29). Nested Moffatt eddies (30) are also present in the cavity corners (not shown). Also, the results reveal that the velocity midway between cavities corresponds to that of the inlet (i.e., parabolic). Therefore, the mixed-cup concentration is defined by eq 13 midway between cavities and can be used to compare the grooved and nongrooved simulations.

Figures 4 and 5 show representative results for the spatial distributions of oxygen and lactate in the bioreactor, respectively. Note the growing boundary layer in the channel and the flat concentration contours in the grooves. The Péclet number is $O(10^{-2})$ in the grooves; thus, transport is expected to be diffusion-limited there. The oscillatory nature of the isoconcentration contours between cavities reflects diffusive transport replenishing (or removing) solute in the absence of chemical reaction.

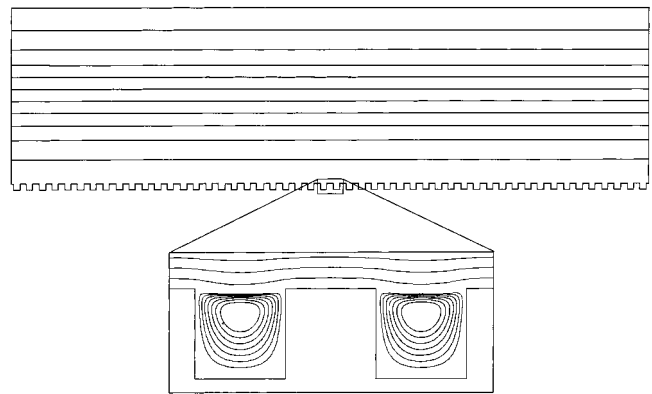


Figure 3. Channel streamlines in this 50-cavity simulation, which are primarily flat ($Q = 2.5$ mL/min). Streamlines for the cavity (inset) show a symmetric cellular flow. The inset also shows the local effect that the cavities have on the channel velocity. This 50-cavity subunit is repeated four times to simulate the entire perfusion chamber. Only 40 cavities of the last subunit are used to give the 190 total cavities in the perfusion chamber.

For illustrative purposes, further results are presented as two case studies. The first case study considers the Sandstrom et al. (14) culture at the three time periods discussed previously. These cultures were performed with medium in equilibrium with high (20%) oxygen. We have shown that, under 5% oxygen concentration, there is greater progenitor cell production (31, 32). The second case study considers cell culture with medium saturated at this lower inlet oxygen concentration of 5%.

Case I: High (20%) Feed Oxygen Concentration.

Figures 6 and 7 show numerical simulations of oxygen and lactate distributions, respectively, in the bioreactor at three stages of the culture period. Each graph contains three lines, representing the concentration at the bottom of the flat-bed chamber and the grooved chamber, as well as the mixed-cup concentration. The mixed-cup concentration curves overlap for the two types of chambers (as in Figure 2); therefore, only one is shown. The overlap of the mixed-cup curves emphasizes the fact that solute consumption (or production) by cells only affects transport on a local scale. Figures 6 and 7 also show how the mixed-cup concentrations at the reactor outlet can be quite deceptive. The minimum oxygen concentration is encountered at the bottom of the last cavity in the reactor and is 76 μ M. This is quite different from the mixed-cup concentration of 186 μ M. Likewise, the maximum lactate concentration is 690 μ M, while the outlet mixed-cup concentration is 40 μ M. Note also that Figures 4 and 5, respectively, are the oxygen and lactate isoconcentration curves for the late culture period of this case study.

Case II: Low (5%) Feed Oxygen Concentration.

Figure 8 shows the oxygen concentration distribution that would be obtained for the cell densities of the Sandstrom et al. (14) cultures for the case of 5% oxygen. The cells are not limited in the early and middle culture phases. However, oxygen limitation will occur at groove 5 in the late phase (data not shown). Using the method described in the next section, the bioreactor can support 7.2×10^6 total cells at a flow rate of 2.5 mL/min ($q_{O_2} = -0.1$ μ mol/(10^6 cells h)). Obviously, oxygen-restricted and eventually oxygen-limited conditions will prevail at lower flow rates or in cultures with higher metabolic requirements. This may also result in higher lactate production as the cells' metabolism becomes more glycolytic.

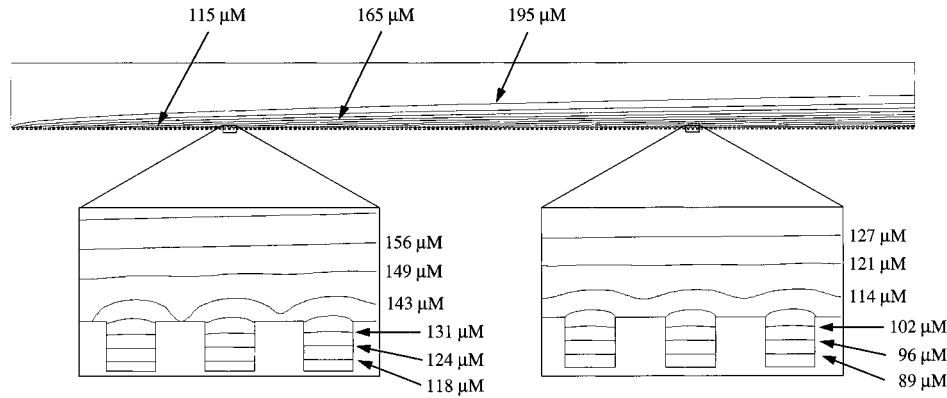


Figure 4. Isoconcentration contours depicting the oxygen distribution in the bioreactor ($Q = 2.5$ mL/min, $q_{O_2}N = -2.0$ μmol of O_2/h). This distribution is characterized by a growing boundary layer in the channel with simple diffusion in the cavities.

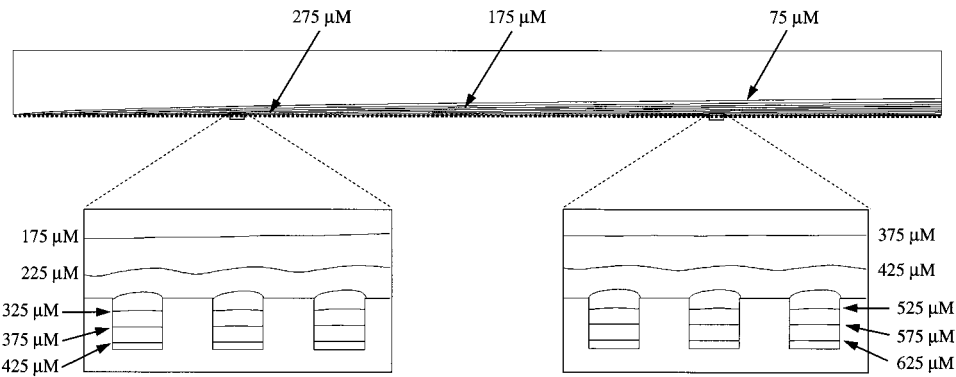


Figure 5. Isoconcentration contours showing the lactate distribution in the bioreactor ($Q = 2.5$ mL/min, $q_{lac}N = +6.0$ μmol of lactate/h). Similar to oxygen, there is a growing boundary layer in the channel with simple diffusion in each cavity. Now, however, upstream production of lactate causes accumulation in downstream cavities.

Correlation for Quickly Calculating the Solute Concentration in the Grooves. As shown in Figure 9, when we compared the concentration difference between the bottom of the flat channel and the bottom of each cavity, e.g. in Figures 6 and 7, we found a linear relationship between the reaction rate and concentration difference. Linear regression of the computational data yields

$$\Delta C_{O_2} = 12.65q_{O_2}N + (1.7 \times 10^{-5}) \quad (14)$$

with a correlation coefficient of nearly 1.0. ΔC_{O_2} is expected to go to zero as $q_{O_2}N$ goes to zero. Comparison of the two terms in eq 14 reveals that the first term is at least 4 orders of magnitude greater than the second; therefore, we can write

$$\Delta C_{O_2} = 370 \frac{q_{O_2}N}{WL} \quad (15)$$

where ΔC_{O_2} is in micromolar and W and L are in centimeters. The reactor length and width have been included here to generalize the relationship. Relating ΔC_{O_2} to the concentration drop due to diffusion through a stagnant cavity

$$\Delta C_i^{diff} = \frac{r_i}{D_i} H_g \quad (16)$$

we have

$$\Delta C_{O_2} = 1.12\Delta C_{O_2}^{diff} \quad (17)$$

Therefore, the actual concentration drop in the cavity is 12% greater than that attributed to diffusion alone.

Examination of the lactate data also revealed a linear relationship over the range studied ($Q = 0.5-2.5$ mL/min, $q_{lac}N = 0.6-6.0$ $\mu\text{mol}/\text{h}$) (data not shown):

$$\Delta C_{lac} = 29.5q_{lac}N + 0.19 \quad (18)$$

with a correlation coefficient of nearly 1. The y -intercept in eq 18 is 2 orders of magnitude smaller than the first term for the lowest lactate production rate considered here ($q_{lac}N = 0.6$ μmol of lactate/h) and can again be neglected. Therefore, we can simplify eq 18 as

$$\Delta C_{lac} = 855 \frac{q_{lac}N}{WL} \quad (19)$$

where ΔC_{lac} is in micromolar and W and L have units of centimeters. Again, comparing to the concentration drop due to diffusion

$$\Delta C_{lac} = 1.12\Delta C_{lac}^{diff} \quad (20)$$

Therefore, the relative concentration drop across the cavity is exactly the same as that for oxygen.

The results of this section can now be used to determine the (local) cell growth environment with minimal computational effort. One simply solves the Graetz problem for the nongrooved system and then determines the solute concentration at the groove bottom using

$$\Delta C_i = 1.12\Delta C_i^{diff} \quad (21)$$

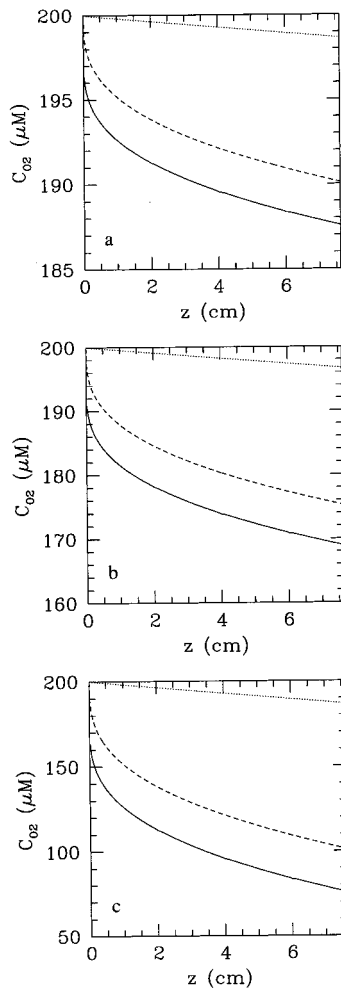


Figure 6. Oxygen not restricting in the bioreactor for the three time points in the study by Sandstrom et al. (14) ($Q = 2.5$ mL/min; $q_{O_2} = -0.1$ $\mu\text{mol}/(10^6$ cells h)), even at the highest cell density. The maximum reported specific oxygen consumption rate was used here to identify possible oxygen limitations. The curves are concentrations at the bottom of the flat (---) and grooved channels (—) and the mixed-cup concentration (···).

Sample results from this procedure are given in Table 2, which presents the maximum total cells that the perfusion chamber can accommodate before oxygen restriction for a variety of flow rates and oxygen consumption rates. This procedure is simple enough that it can be performed on-line, identifying times of transport limitation as they occur.

ΔC_{O_2} as a Function of Cavity Spacing. The effect of decreasing the cavity spacing is examined in this section as a possible means for reducing the total chamber surface area. This translates practically into reduced bench/laboratory space and material costs. Equation 15 can be rewritten as

$$\Delta C_{O_2} = \alpha \frac{q_{O_2} N}{WL} \quad (22)$$

such that α may now vary with cavity spacing (L_g in Figure 1). Results for cavity spacings between 50 and 400 μm are shown in Figure 10. A trend of decreasing α is seen as the cavity spacing decreases. This is expected when one considers the following: (1) the oxygen concentration at the bottom of the flat chamber is expected to decrease with cavity spacing since the number of cells

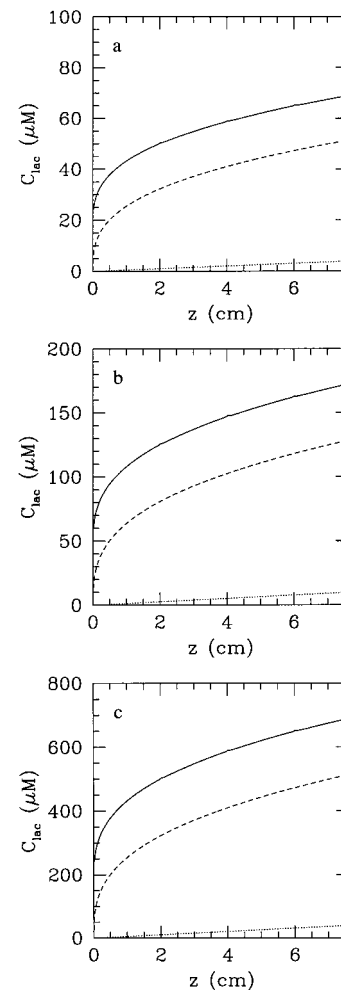


Figure 7. Simulated lactate concentrations during a typical hematopoietic cell culture in the perfusion chamber ($Q = 2.5$ mL/min; $q_{lac} = +0.3$ $\mu\text{mol}/(10^6$ cells h)). The curves are concentrations at the bottom of the flat (---) and grooved channels (—) and the mixed-cup concentration (···).

per reactor surface area increases as L_g decreases and (2) the reaction rate applied at the bottom of the flat channel approaches that of the grooved channel as the cavity spacing decreases. Conversely, as L_g becomes large, the cavities look more and more like point sources when compared to the flat channel. Thus the concentration drop in each cavity must increase relative to the flat channel to give the same total solute flux.

Equation 22, in conjunction with the BEM, can now be used to examine transport in perfusion chambers of various cavity spacings. Figure 11 compares the predicted oxygen concentration at the bottom of three (190-cavity) bioreactors in late culture where the cavity spacing is varied from 50 to 200 μm . For the same number of grooves, these simulations show that the size of the perfusion chamber may be decreased without limiting cell growth under these conditions.

Finally, the maximum number of cells the chambers can accommodate without oxygen restriction is examined using the BEM and Figure 10b. The total number of cells the reactor can support decreases from 33.4×10^6 to 28.2×10^6 cells when the cavity spacing is decreased from 200 to 100 μm . This represents a 16% decrease in total cells for a 25% reduction in total chamber surface area. The chamber can accommodate 25.2×10^6 total cells for a spacing of 50 μm , a 25% reduction in total cells for a

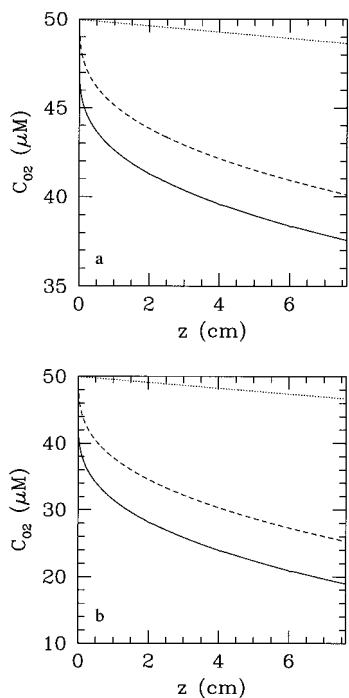


Figure 8. Low (5%) inlet oxygen concentration that does not result in oxygen depletion at the groove bottom for early (a) and middle (b) culture at $Q = 2.5$ mL/min. Simulations suggest that, during the late culture phase, cell growth becomes oxygen-limited. The curves are concentrations at the bottom of the flat (· · ·) and grooved channels (—) and the mixed-cup concentration (— · —).

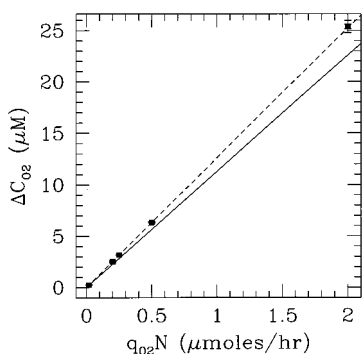


Figure 9. Linear relationship between ΔC_{O_2} and $q_{O_2}N$, which is independent of flow rate since the results for $Q = 0.5, 1.0,$ and 2.5 mL/min shown here overlap. Comparison to ΔC_{diff} (solid line) shows that the primary transport resistance in the cavity is diffusion. An average value is reported in each case, and the error bars represent one standard deviation in the data.

Table 2. Maximum Number of Cells ($\times 10^6$) the Perfusion Chamber Can Maintain without Oxygen Restriction ($C_{O_2} > 10 \mu M$)^a

| q_{O_2} ($\mu\text{mol}/(10^6 \text{ cells h})$) | Q (mL/min) | | |
|--|--------------|------------|------------|
| | 0.5 | 1.0 | 2.5 |
| 0.05 | 39.2 (2.7) | 51.4 (3.6) | 72.0 (5.0) |
| 0.1 | 18.2 (1.3) | 23.9 (1.7) | 33.4 (2.3) |

^a Results are reported as a function of the specific oxygen consumption rate (q_{O_2}) and the volumetric flow rate (Q) for an inlet medium with high (20%) dissolved oxygen concentration. The corresponding number of cell layers present in the grooves is shown in parentheses.

38% reduction in chamber surface area. Also note that the total cells per gross chamber area increases as the cavity spacing is decreased, $1.15 \times 10^6, 1.30 \times 10^6,$ and 1.39×10^6 cells/cm² for 200, 100, and 50 μm , respectively.

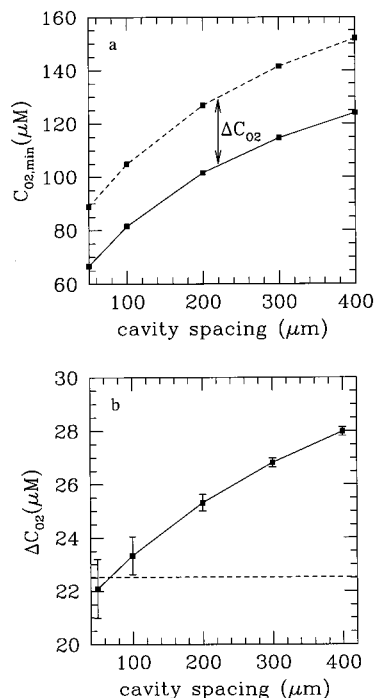


Figure 10. (a) Minimum oxygen concentration in the bioreactor ($C_{O_2,min}$) for the flat-bed (· · ·) and grooved bioreactors (—). (b) Concentration difference (ΔC_{O_2}) increasing with cavity spacing. The dashed line represents the ideal concentration drop in the cavity due to diffusion only, and the error bars represent one standard deviation. ($Q = 2.5$ mL/min; $q_{O_2}N = -2.0 \mu\text{mol/h}$).

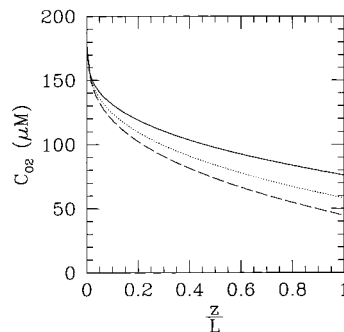


Figure 11. Oxygen concentration at the groove bottoms for $L_g = 200 \mu\text{m}$ (—), $100 \mu\text{m}$ (· · ·), and $50 \mu\text{m}$ (— · —) for late culture. These data were generated using the BEM in conjunction with the results of Figure 10b. These results show that the cavity spacing can be reduced to 50 μm with little effect on the cell growth environment ($Q = 2.5$ mL/min; $q_{O_2}N = -2.0 \mu\text{mol/h}$; 190 cavities).

Discussion

We have developed a differential transport model and implemented a method of numerical integration to simulate the hydrodynamic and solute transport environment in a flat-bed perfusion bioreactor with a grooved bottom. There are no experimental data to compare the simulations to experimental results. However, our simulation findings support the indirect conclusions obtained by Sandstrom et al. (14, 15) that under their experimental conditions the hematopoietic cultures were neither oxygen-limited nor lactate-inhibited. Our analysis shows that the reactor is not oxygen-limited for a variety of feeding protocols. For high (20%) oxygen feed concentration and 20×10^6 cells (late culture), no oxygen limitations are expected for flow rates of 1.0 mL/min or greater. For low (5%) oxygen feed concentration, the culture may become oxygen-limited in the late culture phase, however. The groove spacing may also be decreased to 50 μm without

growth limitation. This reduces not only material costs for manufacturing each chamber but also the laboratory space required for each patient.

While simulated lactate concentrations did not reach local levels inhibitory to hematopoietic cells (assumed > 15 mM (33)), that possibility exists as the cell concentration in the grooves is further increased. Interestingly, groove lactate concentrations can be an order of magnitude higher than the measured outlet concentration.

The above results also suggest two alternatives for bioreactor operation: (1) The perfusion rate may be started at 0.5 mL/min, and increased to 2.5 mL/min as culture proceeds. This would decrease the amount of medium required in the absence of recycle. (2) During the early culture phase, one could feed medium (at 2.5 mL/min) in equilibrium with low (5%) oxygen to enhance progenitor cell expansion and then increase the oxygen content in the medium during culture to enhance cell differentiation (32). The second protocol would reduce axial gradients in oxygen and lactate, yielding a more homogeneous growth environment.

We also showed that there is a 12% increase in the transport resistance due to the presence of cavities at the chamber bottom. This increase was shown to scale with the total flux for oxygen and lactate. The fact that oxygen and lactate transport are affected by the same amount implies that the "12% rule" is solute independent. Therefore, it can be used to determine the distribution of glucose or cytokines, provided their transport can be described according to eq 2. However, the relative increase will change with cavity spacing, as shown in Figure 10b.

There are several possible extensions and improvements of the proposed model. An obvious extension would be to use the Monod equation for oxygen uptake (eq 8) instead of the simplified eq 9. Since q_{O_2} decreases with C_{O_2} below $\sim 10K_m$, this would give a more realistic picture of C_{O_2} values. This, however, will require a substantial modification of the FIDAP simulation code. Further changes in groove geometry and spacing can be readily accommodated without much additional effort. To consider higher cell density operation of the grooved chamber bioreactor, transport within a bed of cells at the bottom of the groove (for more than two to three cell layers) should be considered. This modification will require more computational resources to account for the new domain at the bottom of each cavity.

This bioreactor was observed to have good cell retention for flow rates up to 20 mL/min (14, 15). Balancing the buoyant force on the cells with Stokes' drag results in an estimate of 0.8×10^{-2} cm/s for the local velocity required to drag cells into the flow. The maximum velocity in a cavity is $O(10^{-4}$ cm/s) for a flow rate of 2.5 mL/min (34). For a flow rate of 20 mL/min through the chamber, the velocity at the cavity bottom is still $O(10^{-4}$ cm/s) and only reaches 0.15×10^{-3} cm/s if the cavity is half full. Clearly, the simulations support the fact that the cavities protect cells from the primary flow environment. Also, shear rates at the groove bottom are $O(10^{-3}$ s $^{-1}$) for a flow rate through the chamber of 2.5 mL/min (34). This is well below limits expected to damage these types of cells.

We are currently investigating the use of chaotic advection to minimize the solute gradients that exist between the channel and cavities in the bioreactor. Minimizing these gradients may allow for an increase in the total number of cells the bioreactor can support, through increased local oxygen concentrations at the groove bottom. In this spirit, ongoing experiments reveal

that an unsteady boundary motion (one which breaks steady-state streamlines) can increase mixing in the grooves.

Acknowledgment

This work was supported by National Science Foundation Grant BES-9410751.

Appendix

Application of the BEM to the Graetz problem follows the approach of Ramachandran (25). The BEM employs an integral formulation of the differential equation, which moves the unknowns to the domain boundaries. This reduces the dimensionality of the problem by one, therefore a three-dimensional problem is reduced to a two-dimensional boundary integral, and a two-dimensional problem to evaluation of a line integral. When considering advection-diffusion problems, the BEM typically requires less computational effort and does not suffer from the numerical oscillations encountered when low-order finite difference and finite-element schemes are applied to parabolic differential equations (35). The BEM has the additional benefit of providing gradient values at each nodal position.

The (nondimensional) boundary-value problem governing transport of a dilute solute in a slit in the high Péclet number limit is

$$(1 - y^2) \frac{\partial C}{\partial z} = \frac{\partial^2 C}{\partial y^2} \quad (23)$$

$$\text{B.C. 1: } C|_{z=0} = 1 \quad (24)$$

$$\text{B.C. 2: } \frac{\partial C}{\partial y}|_{y=1} = 0 \quad (25)$$

$$\text{B.C. 3: } \frac{\partial C}{\partial y}|_{y=-1} = Da \quad (26)$$

and Da is the Damköhler number for a zero-order reaction:

$$Da = \frac{kH}{C|_{z=0}D} \quad (27)$$

Application of the BEM to this system begins with multiplication of eq 24 by a weighting function (G) and integration by parts twice:

$$\int_{-1}^1 G(1 - y^2) \frac{\partial C}{\partial z} dy = \left[G \frac{\partial C}{\partial y} \right]_{y=-1}^{y=1} - \left[C \frac{dG}{dy} \right]_{y=-1}^{y=1} + \int_{-1}^1 C \frac{d^2 G}{dy^2} dy \quad (28)$$

Requiring the Laplacian of G to be zero yields two linearly independent solutions for G . Two solutions are required because the concentration and concentration gradient are determined at each boundary point. Applying a forward difference to the convective term

$$\int_{-1}^1 G(1 - y^2) \frac{\tilde{C}}{\Delta z} dy = \int_{-1}^1 G(1 - y^2) \frac{C}{\Delta z} dy + \left[G \frac{\partial C}{\partial y} \right]_{y=-1}^{y=1} - \left[C \frac{dG}{dy} \right]_{y=-1}^{y=1} \quad (29)$$

where \tilde{C} represents the concentration at $z + dz$ and C is the concentration at z .

Numerical implementation is as follows: (1) By dividing the domain into N subelements at z and $z + dz$, eq 29 becomes

$$\sum_{j=1}^N \int_{y_j} G(1 - y_j^2) \frac{\tilde{C}}{\Delta z} dy = \sum_{j=1}^N \int_{y_j} G(1 - y_j^2) \frac{C}{\Delta z} dy + \left[G \frac{\partial C}{\partial y} \right]_{y=-1}^{y=1} - \left[C \frac{dG}{dy} \right]_{y=-1}^{y=1} \quad (30)$$

(2) The concentration is approximated using a cubic polynomial on each y_j . (3) The left-hand side of eq 30 is evaluated using a 10-point Gauss quadrature (36) on each subelement and assembled, with the boundary conditions, into the matrix (\mathbf{L}). (4) The known right-hand side is evaluated on each subelement and assembled into the vector \mathbf{R} . (5) The linear system

$$\mathbf{L} \cdot \tilde{\mathbf{C}} = \mathbf{R} \quad (31)$$

is solved for $\tilde{\mathbf{C}}$ (the vector of concentration point values and gradients ($\partial C/\partial y_j$) at $z + dz$) using LU decomposition (36). This procedure is repeated down the entire reactor length.

References and Notes

- (1) Koller, M. R.; Palsson, B. O. Tissue Engineering: Reconstitution of human hematopoiesis *ex vivo*. *Biotechnol. Bioeng.* **1993**, *42*, 909–930.
- (2) Bertolini, F.; Battaglia, M.; Pedrazzoli, P.; Da Prada, G. A.; Lanza, A.; Soligo, D.; Caneva, L.; Sarina, B.; Murphy, S.; Thomas, T.; della Cuna, G. R. Megakaryocytic progenitors can be generated *ex vivo* and safely administered to autologous peripheral blood progenitor cell transplant recipients. *Blood* **1997**, *89*, 2679–2688.
- (3) Williams, S. F.; Lee, W. J.; Bender, J. G.; Zimmerman, T.; Swinney, P.; Blake, M.; Carreon, J.; Schiling, M.; Smith, S.; Williams, D. E.; Oldham, F.; Van Epps, D. Selection and expansion of peripheral blood CD34⁺ cells in autologous stem cell transplantation for breast cancer. *Blood* **1996**, *87*, 1687–1691.
- (4) Brugger, W.; Heimfeld, S.; Berenson, R. J.; Mertelsmann, R.; Kanz, L. Reconstitution of hematopoiesis after high-dose chemotherapy by autologous progenitor cells generated *ex vivo*. *New Engl. J. Med.* **1995**, *333*, 283–287.
- (5) McAdams, T. A.; Winter, J. N.; Miller, W. M.; Papoutsakis, E. T. Hematopoietic cell culture therapies (Part II): clinical aspects and applications. *Trends Biotechnol.* **1996**, *14*, 387–396.
- (6) Emerson, S. G. *Ex vivo* expansion of hematopoietic precursors, progenitors, and stem cells: The next generation of cellular therapeutics. *Blood* **1996**, *87*, 3082–3088.
- (7) Dexter, T. M.; Allen, T. D.; Lajtha, L. G.; Schofield, R.; Lord, B. I. Simulation of differentiation and proliferation of haemopoietic cells *in vitro*. *J. Cell. Physiol.* **1973**, *82*, 461–74.
- (8) Moore, M. A. S.; Sheridan, A. P. C. Pluripotential stem cell replication in continuous human, prosimian, and murine bone marrow culture. *Blood Cells* **1979**, *5*, 297–311.
- (9) Gartner, S.; Kaplan, H. S. long-term culture of human bone marrow cells. *Proc. Natl. Acad. Sci. U.S.A.* **1980**, *77*, 4756–4759.
- (10) Schwartz, R. M.; Palsson, B. O.; Emerson, S. G. Rapid medium perfusion increases the productivity and longevity of human bone marrow cultures. *Proc. Natl. Acad. Sci. U.S.A.* **1991**, *88*, 6760–6764.
- (11) Koller, M. R.; Bender, J. G.; Miller, W. M.; Papoutsakis, E. T. Expansion of primitive human hematopoietic progenitors in a perfusion bioreactor system with Il-3, Il-6 and stem cell factor. *Bio/Technology* **1993**, *11*, 358–362.
- (12) Palsson, B. O.; Paek, S.-H.; Schwartz, R. M.; Palsson, M.; Lee, G.-M.; Silver, S.; Emerson, S. G. Expansion of human bone marrow progenitor cells in a high cell density continuous perfusion system. *Bio/Technology* **1993**, *11*, 368–372.
- (13) Emerson, S. G.; Clarke, M. F.; Palsson, B. O. Method for *ex vivo* replication of stem cells, for the optimization of human hematopoietic progenitor cell cultures, and for increasing the metabolism, GM-CSF secretion of human stromal cells. U.S. Patent Office Number 5,437,994, Aug 1, 1995.
- (14) Sandstrom, C. E.; Bender, J. G.; Miller, W. M.; Papoutsakis, E. T. Development of novel perfusion chamber to retain nonadherent cells and its use for comparison of human “mobilized” peripheral blood mononuclear cell cultures with and without irradiated stroma. *Biotechnol. Bioeng.* **1996**, *50*, 493–504.
- (15) Sandstrom, C. E.; Bender, J. G.; Miller, W. M.; Papoutsakis, E. T. Effect of CD34⁺ cell selection and perfusion on *ex vivo* expansion of peripheral blood mononuclear cells. *Blood* **1995**, *86*, 958–970.
- (16) Bodoia, J. R.; Osterle, J. F. Finite difference analysis of Plane Poiseuille and Couette flow developments. *Appl. Sci. Res.* **1961**, *A10*, 265–276.
- (17) Randers-Eichhorn, L.; Roscoe, A. B.; Frey, D. D.; Rao, G. Noninvasive oxygen measurements and mass transfer in tissue culture flasks. *Biotechnol. Bioeng.* **1996**, *51*, 466–478.
- (18) Miller, W. M. A kinetic analysis of hybridoma growth and metabolism. Ph.D. Thesis, University of California, Berkeley, 1987.
- (19) Lin, A. A.; Miller, W. M. CHO cell responses to low oxygen: Regulation of oxygen consumption and sensitization to oxidative stress. *Biotechnol. Bioeng.* **1992**, *40*, 505–516.
- (20) Piret, J. M.; Cooney, C. L. Model of oxygen transport limitations in hollow fiber bioreactors. *Biotechnol. Bioeng.* **1991**, *37*, 80–92.
- (21) Graetz, L. Über die wärmeleitfähigkeit von flüssigkeiten. *Ann. Phys. Chem.* **1885**, *25*, 337–357.
- (22) Prins, J. A.; Mulder, J.; Schenk, J. Heat transfer in laminary flows between parallel plates. *Appl. Sci. Res.* **1950**, *A2*, 431–438.
- (23) Sellars, J. R.; Tribus, M.; Klein, J. S. Heat transfer to laminar flow in a round tube or flat conduit—the Graetz problem extended. *ASME Trans.* **1956**, *78*, 441–448.
- (24) Banerjee, P. K.; Butterfield, R. *Boundary Element Methods in Engineering Science*; McGraw-Hill Book Co.: New York, 1981.
- (25) Ramachandran, P. A. *Boundary Element Methods in Transport Phenomena*; Computational Mechanics Publications: Boston, MA, 1994.
- (26) Weiss, R. F.; Florsheim, B. H. Flow in a cavity at low Reynolds number. *Phys. Fluids* **1965**, *8*, 1631–1635.
- (27) Pan, F.; Acrivos, A. Steady flows in rectangular cavities. *J. Fluid Mech.* **1967**, *28*, 643–655.
- (28) Higdon, J. J. L. Stokes flow in arbitrary two-dimensional domains: shear flow over ridges and cavities. *J. Fluid Mech.* **1985**, *159*, 195–226.
- (29) Pozrikidis, C. Creeping flow in two-dimensional channels. *J. Fluid Mech.* **1987**, *180*, 495–515.
- (30) Moffatt, H. K. Viscous and resistive eddies near a sharp corner. *J. Fluid Mech.* **1964**, *18*, 1–18.
- (31) Koller, M. R.; Bender, J. G.; Miller, W. M.; Papoutsakis, E. T. Reduced oxygen tension increases hematopoiesis in long-term culture of human stem and progenitor cells from cord blood and bone marrow. *Exp. Hematol.* **1992**, *20*, 264–270.
- (32) Laluppa, J.; Papoutsakis, E. T.; Miller, W. M. Oxygen tension alters the effects of cytokines on the megakaryocyte, erythrocyte, and granulocyte lineages. *Exp. Hematol.* **1998**, *26*, 835–843.
- (33) Patel, S. J. Improved substrates and feeding protocols for hematopoietic cultures. M. S. Thesis, Northwestern University, 1996.
- (34) Horner, M. Transport in a grooved perfusion flat-bed bioreactor for cell therapy applications. M. S. Thesis, Northwestern University, 1998.
- (35) Wrobel, L. C.; De Figueiredo, D. B. Numerical analysis of convection-diffusion problems using the boundary element method. *Int. J. Num. Methods Heat Fluid Flow* **1991**, *1*, 3–18.
- (36) Press, W. H.; Teukolsky, S. A.; Vetterling, W. T.; Flannery, B. P. *Numerical Recipes in C*, 2nd ed.; Cambridge University Press: Boston, MA, 1992.

- (37) Weast, R. C., Ed. *CRC Handbook of Chemistry and Physics*, 1st student ed.; CRC Press: Boca Raton, FL, 1988.
- (38) Perry, R. H. *Perry's Chemical Engineers' Handbook*, 6th ed.; Green, D. W., Ed.; McGraw-Hill Book Co.: New York, 1984.
- (39) Peng, C.-A.; Palsson, B. O. Determination of specific oxygen uptake rates in human hematopoietic cultures and implications for bioreactor design. *Ann. Biomed. Eng.* **1996**, *24*, 373–381.
- (40) Collins, P. C.; Nielsen, L. K.; Patel, S. D.; Papoutsakis, E. T.; Miller, W. M. Characterization of hematopoietic cell expansion, oxygen uptake and glycolysis in a controlled, stirred-tank bioreactor system. *Biotechnol. Prog.* **1998**, *14*, 446–472.
- (41) Chresand, T. J.; Dale, B. E.; Hanson, S. L. A stirred bath technique for diffusivity measurements in cell matrices. *Biotechnol. Bioeng.* **1988**, *32*, 1029–1036.

Accepted July 20, 1998.

BP980067E